Crystal Growth, Physical and Optical Properties of $TlSr_2Cl_5$ and $TlSr_2Br_5$

Edgar van Loef,[1] Kimberly S. Pestovich,[2] Myles Innis,[1] Jared Schott,[1] Lakshmi Soundara Pandian,[1] Luis Stand,[2] Mariya Zhuravleva,[2, 3] Charles Melcher [2, 3, 4]

[1] Radiation Monitoring Devices 44 Hunt Street, Watertown, MA 02472, USA
[2] Scintillation Materials Research Center University of Tennessee, Knoxville, Knoxville TN, 37996, USA
[3] Department of Materials Science and Engineering University of Tennessee, Knoxville, Knoxville TN, 37996, USA
[4] Department of Nuclear Engineering University of Tennessee, Knoxville, Knoxville TN, 37996, USA

***Abstract* – Small diameter $TlSr_2Cl_5$ and $TlSr_2Br_5$ crystals were grown by the Vertical Bridgman method. X-ray diffraction measurements show that both have the monoclinic crystal structure with space group P21/c. $TlSr_2Cl_5$ and $TlSr_2Br_5$ have a density of 4.14 g/cm^3 and 5.03 g/cm^3, respectively. The effective Z of $TlSr_2Cl_5$ and $TlSr_2Br_5$ is 63.7 and 58.6, respectively. Radioluminescence spectra of $TlSr_2Cl_5$ and $TlSr_2Br_5$ feature a broad emission band peaking at 440 and 445 nm, respectively.**

***Keywords* – A1. DFT Calculations; A1. Radiography; A1. X-Ray Diffraction; A2. Bridgman Technique; B1. Thallium compounds; B2. Scintillator materials.**

1. Introduction

In recent years, there has been a tremendous surge in the discovery of high-density halide scintillators, driven in part by government funded research of substituting low-Z elements in ordinary halide scintillators with thallium, lead, or bismuth ions for High Energy X-Ray Radiography and other Homeland Security applications. Examples of these include Tl_2LaCl_5 [1, 2, 3], Tl_2LaBr_5 [3, 4], Tl_2LiYCl_6 [5, 6], $TlSr_2Cl_5$ [7], $TlSr_2Br_5$ [8], $TlSr_2I_5$ [9, 10, 11], $TlCaCl_3$ [12, 13], $TlCaBr_3$ [13], and $TlCaI_3$ [13, 14].

As a follow up on our previous research into $TlSr_2I_5$ [11], in this paper we report on the crystal growth, physical and optical properties of $TlSr_2Cl_5$ and $TlSr_2Br_5$. Phase diagrams, Differential Scanning Calorimetry and X-Ray Diffraction spectra, and Hygroscopicity, are presented.

2. Experimental Details

A. Crystal Growth

Single crystals of $TlSr_2Cl_5$ and $TlSr_2Br_5$ were grown using the Vertical Bridgman method. The $TlSr_2Cl_5$ crystal was grown off-stoichiometrically (molar fraction $SrCl_2$ = 0.4) at the peritectic melting point of 560°C from TlCl and $SrCl_2$ beads with 99.99% purity. $TlSr_2Br_5$ was grown stoichiometrically from TlBr and$SrBr_2$ beads with 99.99% purity. The beads were subsequently loaded into 16 mm diameter silica ampoules in an argon-purged glovebox at Radiation Monitoring Devices, Inc., and sealed under reduced pressure. After loading the ampoules into the Bridgman furnaces, the molten charge was left to soak for 24 hours at about 25°C above its melting point before the growth run commenced. Crystals were grown at a rate of about 0.5 mm/hour. After the growth run had completed, the crystals were cooled at about 2°C/hour. Crystals were self-seeded from the capillary of the ampoule, and therefore, randomly oriented. Crystalline boules thus obtained were typical 5 to 7 cm long. Note that although both the melt and the boules of $TlSr_2Cl_5$ and $TlSr_2Br_5$ were clear at elevated temperatures (typically > 400°C), the as-grown crystals were somewhat hazy although not completely opaque. Photographs of a $TlSr_2Cl_5$ and $TlSr_2Br_5$ boule are shown in Fig 1.

B. Thermodynamic Properties

Phase diagrams of the systems TlCl – $SrCl_2$ and TlBr – $SrBr_2$ were calculated using FactSage™ [15]. Thermodynamic values for the Standard Enthalpy of Formation ($\Delta H^{\ominus}$) were obtained from density functional theory (DFT) calculations whereas values for the Standard Entropy at 298K ($\Delta S^{\ominus}$) were obtained by Latimer's Method [16].

The thermal properties of $TlSr_2Cl_5$ and $TlSr_2Br_5$ were analyzed using a Seteram Labsys Evo differential scanning calorimetry (DSC) instrument. For a complete description of the system and operation thereof, see Ref. [17]. The hygroscopicity of $TlSr_2Cl_5$ and $TlSr_2Br_5$ was measured using a

Fig 1. Photographs of a boule of $TlSr_2Cl_5$ (left) and $TlSr_2Br_5$ (right).

Surface Measurement Systems Dynamic Vapor Sorption (DVS) instrument. The measurements were performed using single crystals. For more information on the experimental details, see Ref. [18].

C. Powder X-Ray Diffraction

Powder X-ray diffraction (XRD) spectra of $TlSr_2Cl_5$ and $TlSr_2Br_5$ were measured at room temperature and atmospheric pressure. Crystals were ground into a powder inside a nitrogen-filled glovebox at the University of Tennessee, Knoxville, using a mortar and pestle. The powder was then loaded onto a silicon zero-background sample holder and encapsulated by a Kapton film to prevent degradation from moisture during the measurements. For more information about the instrument used, see Ref. [19].

After obtaining the raw XRD data, the HighScore software package was used to match the measured XRD patterns to a published structure [20]. Further phase analysis was performed with the General Structure Analysis System (GSASII), an open-source software package for Rietveld refinement [21].

D. Computational Methods

The band structure of $TlSr_2Cl_5$ and $TlSr_2Br_5$ was calculated using the open source software Burai [22]. For more details, see Ref. [18]. The input data for the calculations were CIF files generated from the refined XRD data for each composition.

E. Optical Characterization

To experimentally determine the band gap, Tauc plots were generated from optical absorbance spectra [23, 24]. The spectra were measured with a Varian Cary 5000 UV-Vis-IR Spectrophotometer using a quartz window sample holder filled with mineral oil. In using the Tauc method, the calculated values of $(\alpha h\nu)^n$ were plotted against $h\nu$ and a linear fit was applied to determine the band gap (α = absorption coefficient, h is Planck's constant, ν = photon's frequency, n = nature of electronic transition). It was assumed that $TlSr_2Cl_5$ and $TlSr_2Br_5$ had direct band gaps (n = 2). The absorption coefficient was calculated from the experimental absorbance data and the Beer-Lambert Law, in which the absorbance is equal to $\log(I/I_0) = -\alpha x \log(e)$ (I_0 is incident light intensity, I is transmitted light intensity, and x is the sample thickness, which was 1.4 mm).

F. Scintillation Characterization

Radioluminescence spectra were recorded at room temperature using a portable X-ray generator operated at 35 kV and 0.1 mA with a tungsten target. Light was dispersed through a PI Acton Spectra Pro SP-2155 monochromator.

Pulse height spectra were recorded using a standard NIM electronics setup with small samples in oil cups that were optically coupled to a super-bialkali (SBA) Hamamatsu R6233-100 photomultiplier tube (PMT). Light yields, expressed in photons per MeV (ph/MeV), were determined by comparing the peak position of the 662 keV full energy peak in the pulse height

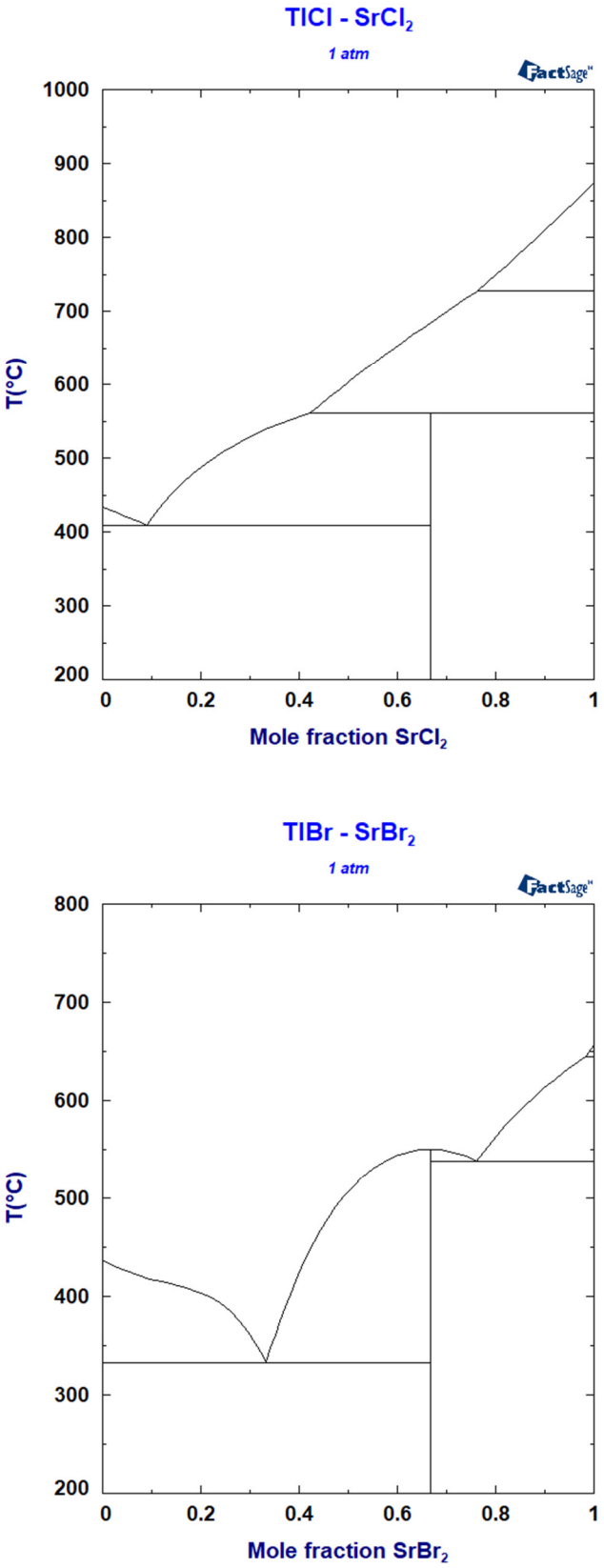

Fig 2. Phase diagrams of the systems TlCl – $SrCl_2$ (top) and TlBr – $SrBr_2$ (bottom) calculated using FactSage™.

spectra with that of a calibrated NaI:Tl crystal, taking into account the quantum efficiency of the PMT. The pulse height spectra were collected using a ^{137}Cs radiation source.

3. Results and discussion

A. Crystal Growth and Differential Scanning Calorimetry

The calculated phase diagrams of the systems TlCl – $SrCl_2$ and TlBr – $SrBr_2$ are shown in Fig 2. The phase diagram of the system TlCl – $SrCl_2$ has been published before [25]. The main difference between the published and calculated phase diagram is the presence of a $SrCl_2$ α → β superionic phase transition [26] in our calculated phase diagram, found at about 730°C. Note that the *$TlSr_2Cl_5$* compound is peritectic and decomposes at about 560°C into TlCl and $SrCl_2$. In contrast, the compound *$TlSr_2Br_5$* does melt congruently and has a melting point of about 560°C.

Note that the eutectic point in the TlBr-rich region of the phase diagram of the TlBr – $SrBr_2$ system is rather depressed at 330°C. We think that this is an artifact of the calculation. The actual eutectic temperature in this region should be much closer to the melting point of TlBr (431°C), as is the case in the TlCl – $SrCl_2$ system.

Differential scanning calorimetry (DSC) data for $TlSr_2Cl_5$ and $TlSr_2Br_5$ are shown in Fig 3. The DSC measurement of a first-to-freeze sample shows one melting and one crystallization peak at 529°C and 562°C, respectively, that matches the reported phase diagram very well. Note that according to the phase diagram, the first-to-freeze section should have the composition *$TlSr_2Cl_5$*, whereas the last-to-freeze section is comprised of the TlCl – $SrCl_2$ eutectic (molar fraction $SrCl_2$ = 0.1).

In the case of $TlSr_2Br_5$, two exothermic peaks and two endothermic peaks are observed. The most intense exothermic (507°C) and endothermic (562°C) peaks are attributed to the crystallization and melting of $TlSr_2Br_5$, respectively. They correspond well with the calculated melting point of $TlSr_2Br_5$ (550°C). The minor exothermic (473°C) and endothermic (479°C) peaks are ascribed to the presence of an impurity, potentially TlBr.

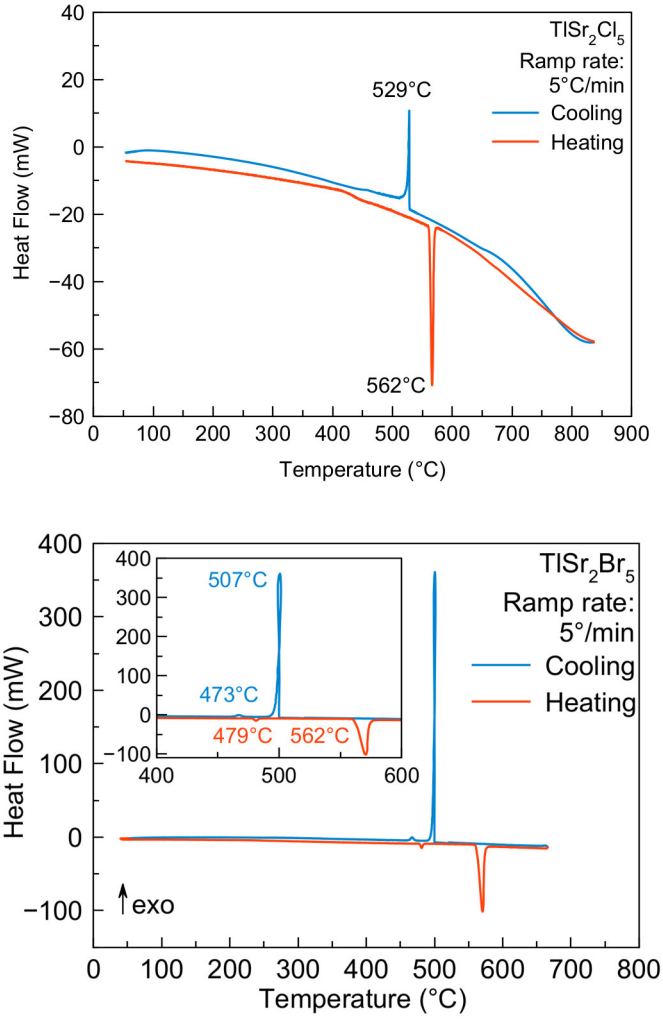

Fig 3. DSC curves for $TlSr_2Cl_5$ (top) and $TlSr_2Br_5$ (bottom).

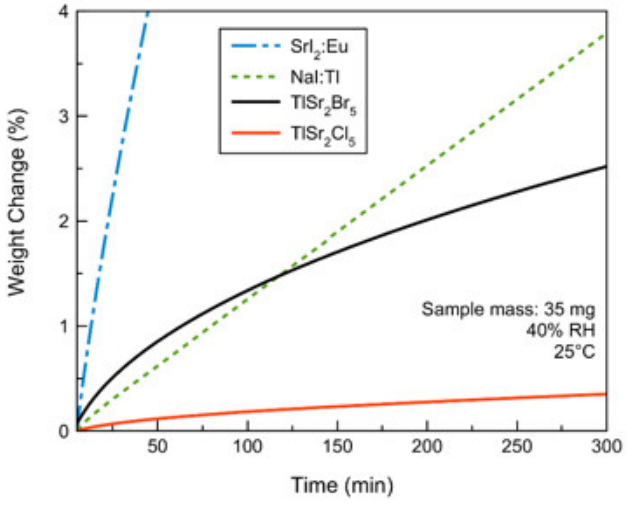

Fig 4. Hygroscopicity of $TlSr_2Cl_5$ and $TlSr_2Br_5$. The data for SrI_2:Eu and NaI:Tl is added for comparison.

B. Hygroscopicity

The relative increase in mass as function of air moisture exposure, i.e., hygroscopicity, of $TlSr_2Cl_5$ and $TlSr_2Br_5$ is shown in Fig 4. To compare, the curves for SrI_2:Eu and NaI:Tl are shown as well. After 5 hours at 40% relative humidity, the final mass percentage increased by approximately 0.5%, 2.5%, and 4%, for $TlSr_2Cl_5$, $TlSr_2Br_5$, and NaI:Tl, respectively, whereas the sample of SrI_2:Eu was 16% degraded. Although the hygroscopicity of $TlSr_2Cl_5$ and $TlSr_2Br_5$ is fairly low, it would be advisable to package both scintillators in airtight and moisture-free containers when used as radiation detectors.

C. X-Ray Diffraction

X-Ray diffraction spectra of $TlSr_2Cl_5$ and $TlSr_2Br_5$ as measured at room temperature are shown in Fig 5. Both

compositions have the monoclinic crystal structure with space group P21/c (14). In the case of $TlSr_2Cl_5$, a secondary phase was observed in a sample of the boule which was confirmed to be TlCl. The TlCl impurity in the first-to-freeze section was 8 weight percent (wt%), whereas a section from the center of the boule contained a TlCl impurity of 55 wt%. The last-to-freeze was pure $SrCl_2$. In contrast, $TlSr_2Br_5$ appears to be phase-pure.

Based on structure and lattice parameters, the calculated density of $TlSr_2Cl_5$ is 4.14 g/cm^3 whereas that of $TlSr_2Br_5$ is 5.03 g/cm^3. The effective Z (Z_{eff}) of $TlSr_2Cl_5$ is 63.7 whereas that of $TlSr_2Br_5$ is 58.6. Although counterintuitive, a lower Z_{eff} for bromides compared to chlorides has been observed before for $LaCl_3$ and $LaBr_3$ [27]. It is related to the relatively higher weight fraction of the bromine ions in ternary bromides compared to chlorine ions in ternary chlorides.

D. Band Structure and Optical Properties

The calculated electronic band structure of $TlSr_2Cl_5$ and $TlSr_2Br_5$ is shown in Fig 6. Both compounds have direct bandgaps of 4.35 eV and 4.04 eV, respectively. Note that the band gaps in Fig 6 are underestimated due to a well-known error in Perdew–Burke-Ernzerhof (PBE) calculations.

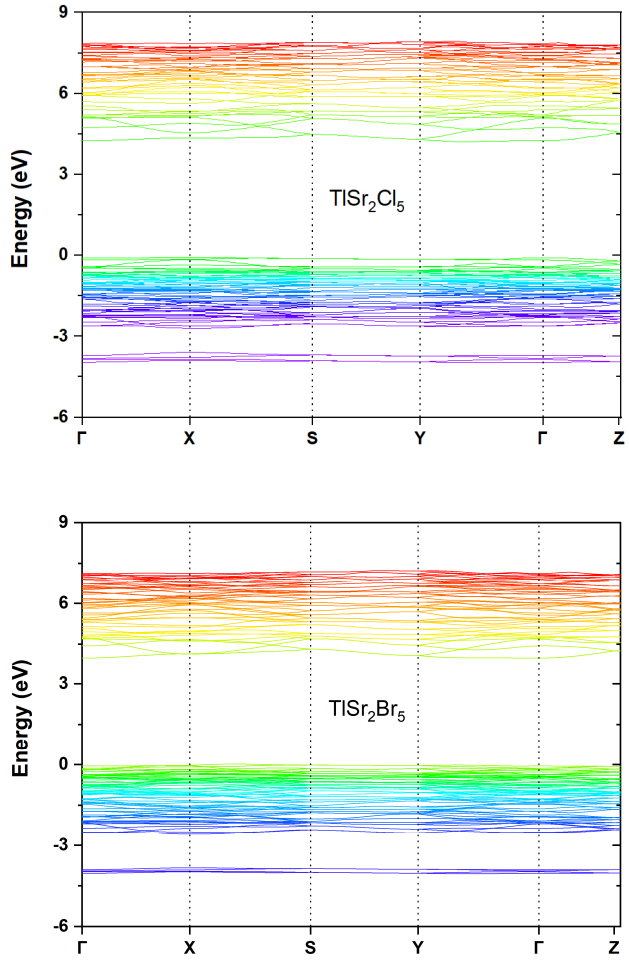

Fig 6. Calculated electronic band structures of $TlSr_2Cl_5$ (top) and $TlSr_2Br_5$ (bottom).

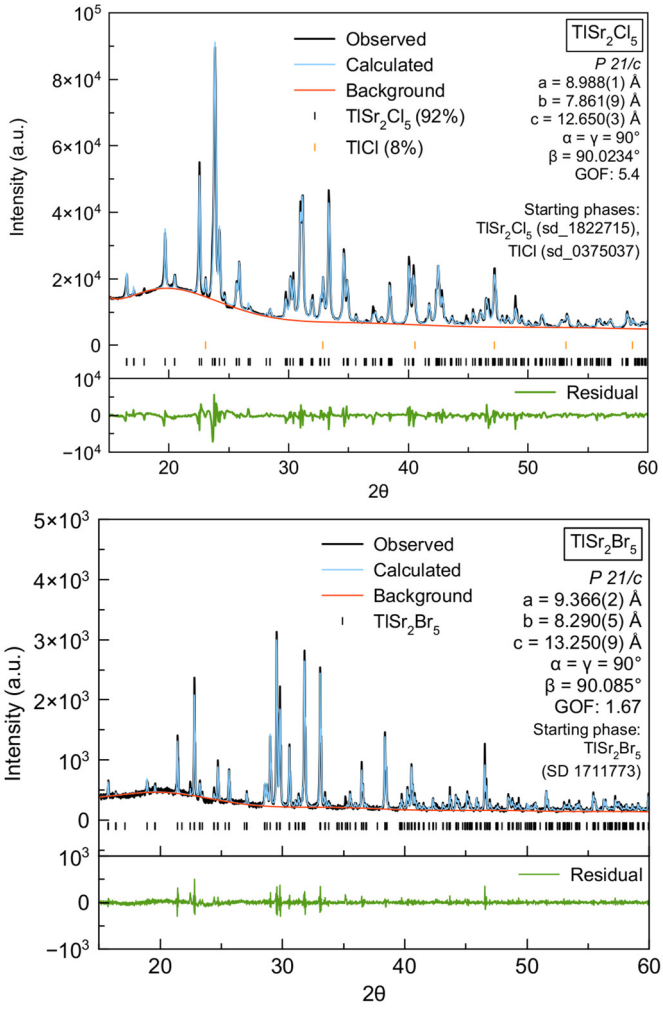

Fig 5. X-Ray diffraction patterns of $TlSr_2Cl_5$ (top) and $TlSr_2Br_5$ (bottom).

The experimentally derived bandgap of $TlSr_2Cl_5$ and $TlSr_2Br_5$ was obtained by extrapolating the last linear segment in the Tauc plot [28] of 1.4 mm thick samples. The Tauc plots of $TlSr_2Cl_5$ and $TlSr_2Br_5$ are shown in Fig 7. In the plot of $TlSr_2Cl_5$ two distinct linear segments can be seen with x-axis intercepts at 3.3 eV and 4.9 eV, respectively. We assume that the value of 3.3 eV is related to the TlCl impurity in the sample used for the measurement (from the first-to-freeze section of the boule), as it matches the published value (3.19 eV) for the bandgap of TlCl well [29]. The value of 4.9 eV corresponds reasonably well with the calculated value for the bandgap of $TlSr_2Cl_5$, when taking into account that the calculated value could be underestimated in this case. In the Tauc plot of $TlSr_2Br_5$ only one linear segment is present with an x-axis intercept of 4.13 eV, which is in very good agreement with the calculated value of 4.04 eV.

The optical absorbance of $TlSr_2Cl_5$ and $TlSr_2Br_5$ as function of wavelength is shown in Fig. 8. As can be seen in the

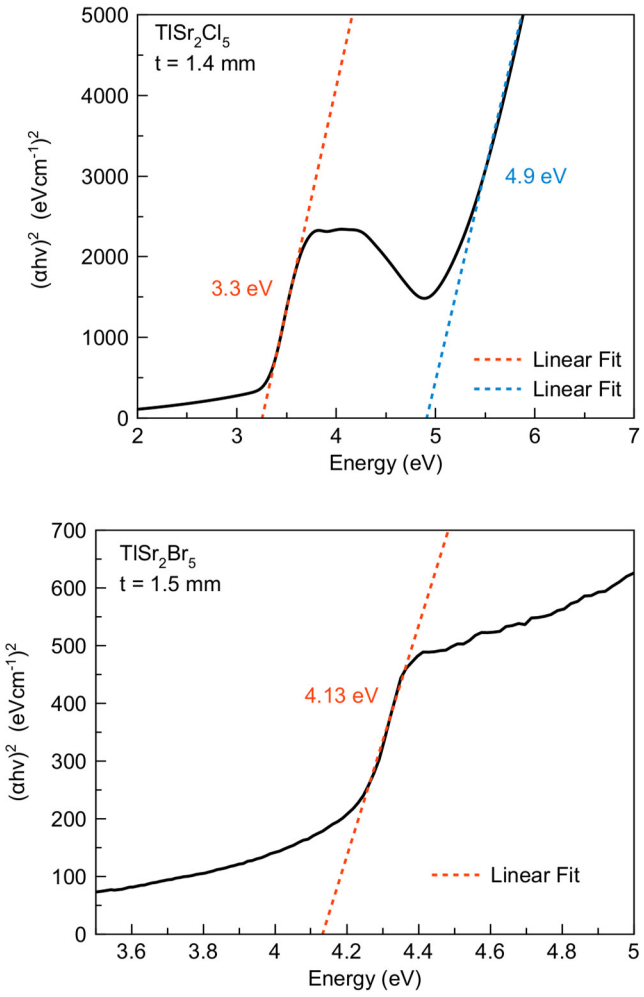

Fig 7. Tauc Plot of $TlSr_2Cl_5$ (top) and $TlSr_2Br_5$ (bottom).

figure, a sharp decrease in the absorbance is noted for $TlSr_2Cl_5$ at about 350 nm (3.54 eV) whereas for $TlSr_2Br_5$ the sharp drop in absorbance is seen at about 400 nm (3.10 eV). These values compare well with the measured bandgaps of $TlSr_2Cl_5$ and $Tl2Sr_2Br_5$.

E. Scintillation Properties

Radioluminescence spectra of $TlSr_2Cl_5$ and $TlSr_2Br_5$ are shown in Fig. 9. The spectra feature a broad emission band peaking at 440 nm and 445 nm, respectively for $TlSr_2Cl_5$ and $TlSr_2Br_5$, which is attributed to thallium and/or host (self-trapped exciton) emission. A similar broad emission was reported for $TlCdCl_3$ and $TlMgCl_3$, which was speculated to relate to self-trapped excitons [30, 31]. Note that the typical red-shift that is observed between chloride and bromide crystals is almost absent for $TlSr_2Cl_5$ and $TlSr_2Br_5$. However, the widths of the emissions are different. $TlSr_2Cl_5$ has a broader emission. Broadening of luminescence bands may indicate strong electron-phonon coupling [32]. Therefore, broadening of the emission of $TlSr_2Cl_5$ compared to $TlSr_2Br_5$ may indicate

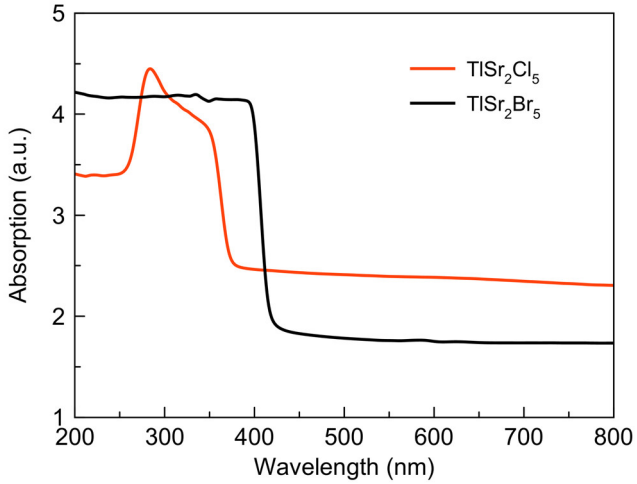

Fig. 8. Optical absorbance of $TlSr_2Cl_5$ and $TlSr_2Br_5$.

different intrinsic emission mechanisms, which may be explored in future studies.

The light yield of $TlSr_2Cl_5$ and $TlSr_2Br_5$ was determined to be 17,000 ph/MeV and 45,000 ph/MeV, respectively. These values are very similar to those reported by Arai *et al.* [7] and Rooh *et al.* [8].

4. Conclusion

In this work we reported on the crystal growth, physical and optical properties of $TlSr_2Cl_5$ and $TlSr_2Br_5$. Crystals were grown by the Vertical Bridgman method. X-ray diffraction measurements show that $TlSr_2Cl_5$ and $TlSr_2Br_5$ have the monoclinic crystal structure with space group P21/c and densities of 4.14 g/cm^3 and 5.03 g/cm^3, respectively. The effective Z of $TlSr_2Cl_5$ is 63.7 whereas that of $TlSr_2Br_5$ is 58.6. Radioluminescence spectra of $TlSr_2Cl_5$ and $TlSr_2Br_5$ feature a broad emission band peaking at 440 and 444 nm, respectively.

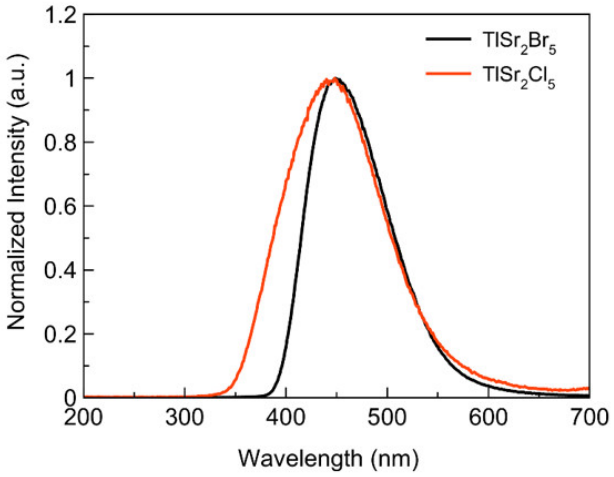

Fig. 9. Radioluminescence spectra of $TlSr_2Cl_5$ and $TlSr_2Br_5$.

In a future work, we plan to investigate the effect of Eu^{2+} doping on the scintillation properties of $TlSr_2Br_5$ and compare its scintillation properties with those of $RbSr_2Br_5$:Eu.

5. Acknowledgements

This material is based upon work supported by the U.S. Department of Homeland Security under Grant Award Number 20CWDARI00036-01-00 and the Department of Energy National Nuclear Security Administration through the Nuclear Science and Security Consortium under Award Number DE-NA0003996. The views and conclusions contained in this document are those of the authors and should not be interpreted as necessarily representing the official policies either expressed or implied, of the U.S. Department of Homeland Security. XRD was performed at the Institute for Advanced Materials & Manufacturing (IAMM) Diffraction Facility, located at the University of Tennessee, Knoxville.

6. References

[1] H. J. Kim, Gul Rooh, and Sunghwan Kim, "Tl_2LaCl_5 (Ce^{3+}): New Fast and Efficient Scintillator for X- and γ-ray detection", 2016, arXiv 1607.05486.

[2] R. Hawrami, E. Ariesanti, H. Wei, J. Finkelstein, J. Glodo, K. S. Shah, "Tl_2LaCl_5:Ce, high performance scintillator for gamma-ray detectors", Nucl. Instr. Meth. Phys. Res. A 869 (2017) 107 – 109.

[3] Edgar V. van Loef, Guido Ciampi, Urmila Shirwadkar, Lakshmi Soundara Pandian, Kanai S. Shah, " Crystal growth and scintillation properties of Thallium-based halide scintillators", J. Crystal Growth 532 (2020) 1225438.

[4] H. J. Kim, Gul Rooh, Arshad Khan, Sunghwan Kim, "New Tl_2LaBr_5: Ce^{3+} Crystal Scintillator for γ-Rays Detection", 2016, arXiv 1612.02918.

[5] R. Hawrami , E. Ariesanti, H. Wei , J. Finkelstein, J. Glodo, and K. Shah, "Tl_2LiYCl_6: Large Diameter, High Performing Dual Mode Scintillator", Crystal Growth & Design 17 (2017) 3960 – 3964.

[6] Gul Rooh, H. J. Kim, H. Park, Sunghwan Kim, "Crystal growth and scintillation characterizations of Tl_2LiYCl_6: Ce^{3+}", J. Crystal Growth 459 (2017) 163 – 166.

[7] Miki Arai, Keisuke Takahashi, Yutaka Fujimoto, Masanori Koshimizu, Takayuki Yanagida, Keisuke Asai, "$TlSr_2Cl_5$: New intrinsically activated crystalline scintillator", Rad. Meas. 134 (2020) 106328.

[8] Gul Rooh, Arshad Khan, H.J. Kim, H. Park, Sunghwan Kim, "$TlSr_2Br_5$: New intrinsic scintillator for X-ray and ɣ-ray detection", Opt. Mat. 73 (2017) 523 – 526.

[9] H. J. Kim, Gul Rooh, Arshad Khan, H. Park, Sunghwan Kim, "The Characterization of new Eu^{2+} doped $TlSr_2I_5$ Scintillator Crystals", 2017, arXiv 1709.04975.

[10] H.J. Kim, Gul Rooh, Arshad Khan, H. Park, Sunghwan Kim, "Scintillation performance of the $TlSr_2I_5$ (Eu^{2+}) single crystal", Opt. Mat. 82 (2018) 7 – 10.

[11] Lakshmi Soundara Pandian, Matthew Loyd, Mao-Hua Du, Edgar van Loef, Guido Ciampi, Luis Stand, Mariya Zhuravleva, Merry Koschan, Jarek Glodo, Charles Melcher, Kanai Shah, "$TlSr_2I_5$:Eu^{2+} - A new high density scintillator for gamma-ray detection", Nucl. Instr. Meth. Phys. Res. A 988 (2021) 164876.

[12] Arshad Khan, Gul Rooh, H.J. Kim, H. Park, Sunghwan Kim, "Intrinsically activated $TlCaCl_3$: A new halide scintillator for radiation detection", Rad. Meas. 107 (2017) 115 – 118.

[13] E. Van Loef *et al*., "Crystal Growth, Density Functional Theory, and Scintillation Properties of $TlCaX_3$ (X = Cl, Br, I)," IEEE Trans. Nucl. Sci., doi: 10.1109/TNS.2023.3258065.

[14] R. Hawrami, E. Ariesanti, H. Wei, J. Finkelstein, J. Glodo, K. S. Shah, "Intrinsic scintillators: $TlMgCl_3$ and $TlCaI_3$", J. Crystal Growth 475 (2017) 216-219.

[15] http://www.factsage.com

[16] P. J. Spencer, ""Estimation of thermodynamic data for metallurgical applications", Thermochimica Acta, vol. 314, pp. 1-21, Nov. 1998

[17] Edgar van Loef, Urmila Shirwadkar, Lakshmi Soundara Pandian, Guido Ciampi, Luis Stand, Mao-Hua Du, Merry Koschan, Matthew Loyd, Mariya Zhuravleva, Charles Melcher, Kanai Shah, "Crystal growth, density functional theory, and scintillation properties of Tl_3LnCl_6:Ce^{3+} and $TlLn_2Cl_7$:Ce^{3+} (Ln = Y, Gd)", Nucl. Phys. Res. A., vol. 995, pp. 165-148, Apr. 2021.

[18] Edgar van Loef, Lakshmi Soundara Pandian, Nathaniel Kaneshige, Guido Ciampi, Luis Stand, Daniel Rutstrom, Yauhen Tratsiak, Mariya Zhuravleva, Charles Melcher, Kanai S. Shah, "Crystal Growth, Density Functional Theory, and Scintillation Properties of $TlCaX_3$ (X = Cl, Br, I)", IEEE Trans. Nucl. Sci. (2023), doi:10.1109/TNS.2023.3258065

[19] Edgar van Loef, Lakshmi Soundara Pandian, Guido Ciampi, Luis Stand, Mao-Hua Du, Daniel Rutstrom, Mariya Zhuravleva, Charles Melcher, Kanai Shah, "Crystal growth, density functional theory, and scintillation properties of $TlMgX_3$ (X = Cl, Br, I)", Chem. Phys., vol. 558, pp. 11535, April 2022.

[20] T. Degen, M. Sadki, E. Bron, U. König, and G. Nénert, "The HighScore suite", Powder Diffraction, vol 29, pp. S13-S18, 2014.

[21] B. H. Toby and R. B. Von Dreele, "GSASII: the genesis of a modern open-source all-purpose crystallography software packaged", J. Appl. Crystall., vol. 46, pp. 544-549, 2013.

[22] https://nisihara.wixsite.com/burai/home

[23] A. Dolgonos, T. O. Mason, and K. R. Poeppelmeier, "Direct optical band gap measurement in polycrystalline semiconductors: A critical look at the Tauc method," J. Solid State Chem., vol. 240, pp. 43-48, 2016.

[24] J. Tauc, R. Grigorovici, and A. Vancu, "Optical properties and electronic structure of amorphous germanium," Phys. Stat. Sol. (b), vol. 15, no. 2, pp. 627-637, 1966.

[25] von H. Fink und H.-J. Seifert, "Über die Systeme des Europium(II)- und Strontiumchlorids mit Alkalimetallchloriden und Thalliumchlorid", Z. anorg. allg. Chem. 466 (1980) 87 – 96.

[26] Stephen Hull, Stefan T. Norberg, Stefan T. Norberg, Istaq Ahmed, Sten Eriksson, Chris E. Mohn, "High temperature crystal structures and superionic properties of $SrCl_2$, $SrBr_2$, $BaCl_2$ and $BaBr_2$", J. Solid State Chem. 184 (2011) 2925 – 2935.

[27] E.V.D. van Loef, P. Dorenbos, and C.W.E. van Eijk, "High-energy resolution scintillator: Ce^{3+} activated $LaBr_3$", Appl. Phys, Lett. vol. 79, no. 10, pp. 1573-1575, 2001.

[28] J. Tauc, R. Grigorovici, and A. Vancu, "Optical properties and electronic structure of amorphous germanium," *physica status solidi (b),* vol. 15, no. 2, pp. 627-637, 1966.

[29] A.D. Brothers and D.W. Lynch, "Optical Properties of AgCl, AgBr, TlCl, and TlBr under Hydrostatic Pressure", Phys. Rev., vol. 180, no. 3, pp. 911-918, 1969.

[30] Y. Fujimoto, M. Koshimizu, T. Yanagida, G. Okada, K. Saeki, and K. Asai, "Thallium magnesium chloride: A high light yield, large effective atomic number, intrinsically activated crystalline

scintillator for X-ray and gamma-ray detection," Jap. J. Appl. Phys., vol. 55, no. 9, p. 090301, 2016.
[31] Y. Fujimoto, K. Saeki, T. Yanagida, M. Koshimizu, and K. Asai, "Luminescence and scintillation properties of $TlCdCl_3$ crystal," Radiation Measurements, vol. 106, pp. 151-154, 2017.
[32] P. A. Rodnyi, Physical processes in inorganic scintillators. CRC press, 2020.